AIChE InterScience DISCOVER SOMETHING GREAT

BIOENGINEERING, FOOD, AND NATURAL PRODUCTS

Numerical Modeling of a High Pressure Thawing Process of a Biomaterial

A. Ousegui, A. LeBail, and M. Havet
UMR GEPEA (UA CNRS 6144), ENITIAA, Rue de la Géraudière BP 82225, 44322 Nantes, Cedex 03, France

DOI 10.1002/aic.11391
Published online December 17, 2007 in Wiley InterScience (www.interscience.wiley.com).

A numerical model for predicting temperature and velocity fields during conjugate heat transfer in a high pressure (HP) (~200 MPa) thawing process presented. This model considers the apparent specific heat formulation to solve the energy equation with phase change and the shift approach to extrapolate thermophysical properties at HP. It does not require the adjustement of the convective heat transfer coefficient. The compressible flow of water in the HP vessel is calculated. It is shown that the fluid motion is dominated by forced convection in the compression phase and by natural convection during the holding phase. A very good agreement between numerical and experimental results is obtained. Additional simulations carried out at various pressures permit to assess the influence of the pressure level on the thawing time. The analysis of the phase change inside the food and of the velocity field inside the vessel clearly demonstrates the great potential of this model to optimize this HP process at an industrial scale. © 2007 American Institute of Chemical Engineers *AIChE J,* 54: 544–553, 2008
Keywords: phase change, heat transfer, CFD

Introduction

High pressure (HP) processes at sub zero freezing temperatures are attracting research efforts. HP assisted freezing or thawing are innovative processes with a great potential for the food industry. They are mainly based on the decreasing of the freezing temperature of water against the pressure. The shift of the freezing temperature was firstly pointed out by Bridgmann.[1] According to Kalichevsky et al.[2] and Urrutia et al.,[3] this property could permit to achieve rapid thawing or freezing of food under HP, suggesting the possibility of new applications in the area of food process. Different processes can be investigated according to the pathway on the phase change diagram (Figure 1).

Pressure assisted freezing (P.A.F) (ABCD in Figure 1) has been applied to food systems. Several authors have investigated the thermal aspects as well as the impact on food quality. For example, Fuchigami and Teramoto[4] showed a reduction of the drip losses accompanied by changes in texture.

Correspondence concerning this article should be addressed to M. Havet at havet@enitiaa-nantes.fr.

As mentioned by Zaho et al.[5] and Hendrickx et al.,[6] Pressure assisted thawing (P.A.T) (DCBA in Figure 1) might also result in a reduction of the drip losses and in a modification of the enzymatic activity.

Pressure shift freezing (P.S.F) (AEFG in Figure 1) was the subject of many studies. Most of them focus on the advantageous effects on texture and structure of products. P.S.F is characterized by a uniform ice nucleation permitted to obtain products that look like fresh samples. Minimal differences in tissue damage were observed between center and surface of products for large meat pieces by Martino et al.[7] and Zhu et al.[8]

Pressure induced thawing (P.I.T) (GFEA in Figure 1) is the other technique in HP area. According to Knorr et al.,[9] most studied realized so far concluded that the major advantage of this technique is the reduction of treatment time. More details on this HP process and potential applications are available in the literature.[10–12]

Several studies on modeling of HP process are available. These studies can be classified in two main categories according to whether they take into account or not phase change phenomena.

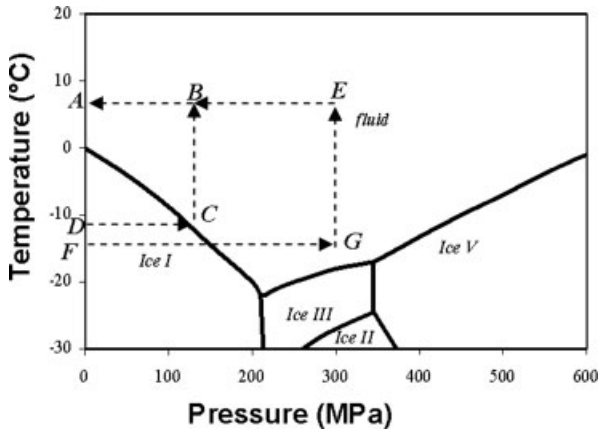

Figure 1. Process pathways for HP assisted thawing.

Studies focusing on modeling of HP process without phase change mainly dealt with enzymatic inactivation. Denys et al.[13] studied the transient evolution of the temperature field during the HP treatment applied to apple juice and tomato puree. They solved only the equation of energy (diffusive model) by taking into account the compression and release steps. They coupled this model with an enzymatic inactivation law. The results showed the strong influence of temperature changes during compression and decompression on the local enzymatic activity distribution after processing. Hartmann and Delgado[14] also studied the inactivation of enzymes in an aqueous solution during HP process. By solving the energy and Navier-Stokes equations, they showed that the uniformity of the treatment could be disturbed by the viscosity of the solution, the size of the HP vessel and the diffusive transfers. This work demonstrated the importance of studying the velocity distribution and the fluid motion to evaluate the global inactivation in a fluid domain. Undergoing HP treatments, Hartmann[15] studied the heating effects and dynamic HP treatment on water. The model allowed a space-time analysis of the velocity and temperature profiles. They confirmed the temperature increase during the compression phase, for which forced convection was prevalent. During the pressure holding phase of the process, free convection became the prevalent phenomenon for fluid motion. Hartmann et al.[16] modeled temperature changes during compression and decompression, taking into account the compressibility parameter.

Studies focusing on modeling of HP process with phase change mainly concerned thawing and freezing processes under HP. Schluter et al.[17] modelled PAF of a potato sample installed in a HP vessel. The geometry of the sample was a cylinder with a small diameter (1 cm), so that a one-dimensional model was considered. A finite difference model was designed assuming a purely conductive heat transfer between the wall of the vessel and the sample. A regression of the values of thermal conductivity and specific heat obtained at atmospheric pressure were used and adjusted to obtain a good fit between calculated and experimental temperature profiles. Sanz and Otero[18] studied the freezing of an agar gel and of water. They focused on the compression phase and took into account the supercooling caused by the pressure release. The mathematical model predicted the freezing time by adding the durations of three stages: cooling, pressure shift, and temperature equilibration. This approach did not permit to obtain the temperature variation after supercooling and the model was then limited to reproduce only the pressure release phase. Moreover, a global heat transfer coefficient between the wall of the vessel and the sample was adjusted to obtain a good fit between experiments and calculations. Kowalczyk et al.[19] modeled the freezing of water under HP, they reformulated the conservation equations (mass, momentum, and energy) by using the Enthalpy-Porosity formulation of Bennon and Incropera[20] to model the liquid–solid transition. The authors mentioned the importance of the convection on the formation and the development of ice. They mentioned a reduced ice formation in high velocity zones. Fore pure water, this numerical approach is suited and other melting front tracking techniques could also be employed.[21] For aqueous solutions and especially for food systems, melting occurs on a range of temperature and the apparent specific heat formulation is still suited.[22]

Chourot et al.[23] modeled the thawing of an aqueous solution (4% NaCl) at various pressures (P_{atm}, 100 and 150 MPa). A finite differences method was used in cylindrical coordinates (1D). A Crank Nicholson scheme was considered to solve the heat diffusion equation. The model, based on the method of the apparent specific heat, took into account the change of the temperature and the latent heat of fusion according to the pressure. A global convective heat transfer coefficient was considered (natural convection) in the annular gap located between the sample and the vessel wall. This coefficient was calculated by optimizing the empirical parameters of relations from the literature. Denys et al.[24] modeled heat transfer during freezing and thawing of a food models (Tylose), which properties were extrapolated starting from correlations of the literature at atmospheric pressure. Once again, the convective heat transfer coefficient between the sample and the vessel was assumed constant and was used to adjust the model. A method of correction of enthalpy was used and the transfer by convection because of the pressurizing fluid was taken into account thanks to an apparent conductivity. The authors had to adjust the value of this apparent conductivity to obtain a good fit between experimental and calculated temperatures. Same authors[25] improved the previous model in including the evolution of the latent heat of melting according to the pressure. However, they also had to adjust the convective heat transfer coefficient in the pressurization fluid to obtain a good agreement between computed and experimental data.

The analysis of these works shows that the models developed in the case of HP process with phase change focused only on the solid domain (food sample). As an overall heat transfer coefficient were adjusted to fit experimental data, no real effort was done to take into account the free convection flow that developed between the food and the vessel in the pressurization fluid. Therefore, all these studies were unable to make any extrapolation outside the experimental domain in which the models were validated. This work aims at answering this aspect by developing a model for HP induced thawing process taking into account conjugate heat transfer in the fluid and solid domains. It is planed to accommodate the following parameters:

- temperature change of the pressurization medium during the compression phase.
- dependence of the thermal conductivity, the specific heat, the viscosity, the density, and the thermal expansion of the pressurization fluid with pressure and temperature.

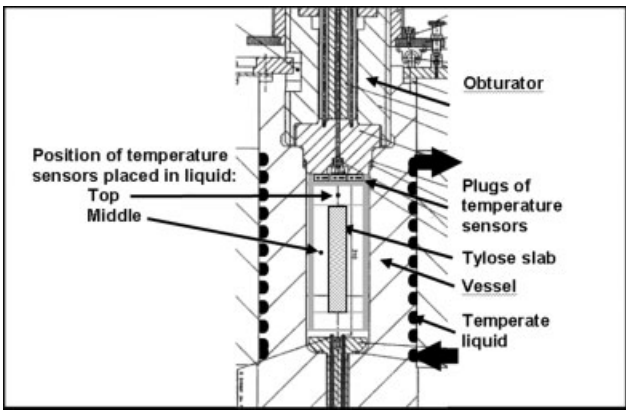

Figure 2. Scheme of the HP vessel.

• forced convection phenomenon occurring during the compression phase, and natural convection during pressure holding phase.

• dependence of the melting temperature and of the latent heat of fusion with pressure.

Materials and Methods

Tylose (methylcellulose gel) was used as a food model. Tylose slabs (MADI S.n.c., Italy), with external dimensions $100 \times 200 \times 25$ mm^3, were vacuum packed in polyethylene bags. Experiments were carried out on a vessel (ACB Pressure System– Nantes, France) that had an inner diameter of 120 mm and an internal height of 300 mm (Figure 2). A specific lift system was developed to manipulate the obturator and the food sample. A circulating glycol bath was connected to the HP vessel to maintain its temperature constant. Water was used as fluid of pressurization. The increase of pressure was produced by injection of pressurized fluid inside the HP vessel. The HP system was composed of a pump (power 4 kW) ensuring a maximum volumetric flow rate of 3.33×10^{-6} m^3 s^{-1}.

The obturator allowed the passage of 5 calibrated thermocouples (K-type). Three thermocouples (Ø 1 mm, K-type) were positioned into the sample at the surface, at the quarter and in the middle on three different tylose slabs (Figure 3). The exact location of the thermocouples was obtained at the end of the experience after cutting the slabs. The two other thermocouples (Ø 0.3 mm, K-type) were installed in the vessel, at a "top" location over the sample and at a "middle" location at equal distance between the wall and the sample (Figure 2).

A data logger (SA32, AOIP, France) was used to record the temperature and the pressure during the process. Data acquisition frequency was every 5 s during thawing treatment. Three experiments were conducted at 200 MPa in order to validate the model.

Mathematical model

The conjugate heat transfer model should consider two zones: the fluid domain, i.e., water as it is the pressurization medium and the food sample.

Fluid domain

To simulate this process, the equations of fluid dynamics applied to Newtonian and compressible fluid was used: continuity (1) momentum (2) and energy Eq. 3:

$$\frac{\partial \rho}{\partial t} + \nabla \cdot \left(\rho \vec{V}\right) = 0 \tag{1}$$

$$\frac{\partial \left(\rho \vec{V}\right)}{\partial t} + \vec{\nabla} \cdot \left(\rho \vec{V} \cdot \vec{V}^T\right) = \vec{\nabla} . \tau - \vec{\nabla} p + \rho \vec{g} \tag{2}$$

$$\tau = \mu\left(\vec{\nabla}\vec{V} + \vec{\nabla}\vec{V}^T\right) - \frac{2}{3}\mu\left(\nabla \cdot \vec{V}\right)\bar{I}$$

$$\frac{\partial \rho H}{\partial t} + \vec{\nabla} \cdot \left(\rho \vec{V} \cdot H\right) = \vec{\nabla} . \left(\lambda \vec{\nabla} T\right) + S_{\text{fluid}} \tag{3}$$

As water was considered as a compressible fluid, Boussinesq approximation applied at atmospheric pressure[26] was no more usable. The equation of state of water, especially the density, proposed by Chizhov and Nagornov[27] was implemented in the model. Their equation was valid in the consid-

	Sensors	x (mm)	y (mm)	z (mm)	Position of sensors in tylose
TEST 1	T1	60	0.0	100	
	T2	46	7.5	100	
	T3	35.5	12.5	100	
TEST 2	T1	59	0	100	
	T2	42	7.5	100	
	T3	28.5	6.5	100	
TEST 3	T1	64	1	72.8	
	T2	51.5	12	72.8	
	T3	35	5	100	

Figure 3. Thermocouple locations for each experiment.

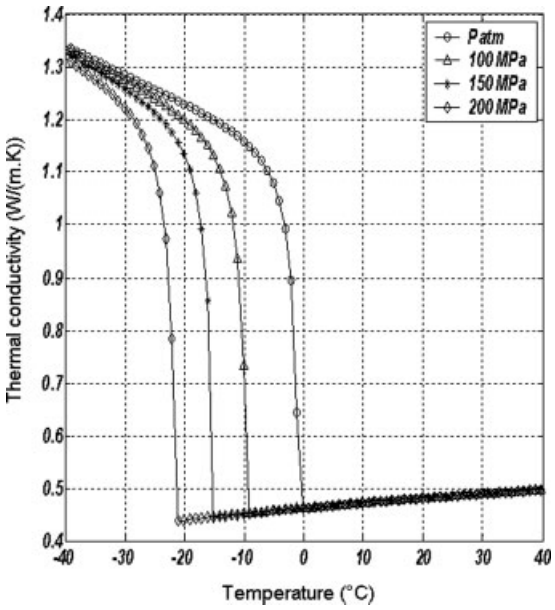

Figure 4. Evolution of the thermal conductivity of Tylose according to the pressure and the temperature.

ered pressure and temperature ranges. Pressure and temperature dependent relations of the specific heat capacity, viscosity proposed by Schluter,[28] and thermal conductivity of water proposed by Tanishita et al.,[29] were used for the fluid domain. All the expressions are given in Appendix.

The source term S_{fluid} introduced in the energy equation permitted to consider the heating of water during the compression phase. It was deduced from the classical thermodynamic relations between the partial derivatives of entropy and enthalpy. By considering an isentropic compression, partial derivatives of temperature and pressure are linked Eq. (4). The heat variation is then easily calculated Eq. (5) and the volumetric source is term directly deduced Eq. (6).

$$dT = \frac{T\upsilon\alpha}{C_{\text{p}}}dp \tag{4}$$

$$\delta Q = \rho C_{\text{P}} dT = \alpha T dp \tag{5}$$

$$S_{\text{fluid}} = \frac{\delta Q}{dt} = \alpha T \frac{dp}{dt} \tag{6}$$

The thermal dilatation of water α (K^{-1}) was calculated from a correlation given by Chizhov and Nagornov[27] (see Appendix).

Solid domain

The apparent specific heat formulation was chosen in the energy equation to model the melting of tylose:

$$\rho\left(C_{\text{p}}\right)_{\text{app}} \frac{\partial T}{\partial t} = \nabla \cdot (\lambda \nabla T) + S_{\text{solid}} \tag{7}$$

The apparent heat capacity and thermal conductivity were evaluated at atmospheric pressure using additive models.[26] They are based on the contribution of each component: dry matter, water, and ice. At HP, the ice ratio was determined by applying a shift approach on Miles equation[30] Eq. (8). This approach consists in calculating the ice ratio according to the shift of the melting temperature Eq. (9). More details are given by Denys et al.[24] and by Otero et al.[31] The resulting evolution of apparent heat capacity and thermal conductivity with pressure are shown on Figures 4 and 5.

$$X_{\text{ice}}(P,T) = (X_{\text{wt}} - X_{\text{b}}) \cdot \left(1 - \frac{T_{m,\text{Patm}}}{T + \left(T_{m,\text{Patm}} - T_{m,P}\right)}\right) \tag{8}$$

$$T_{m,P} = T_{\text{m,Patm}} - 0.072192P - 0.000155P^2 \tag{9}$$

Whereas the temperature of the water increased, the temperature of the food sample was decreasing during the compression phase. In fact, while ice existed in the product, its temperature slid along the phase change line without crossing it. This phenomenon was taken in a previous work by readjusting the temperature.[24] We preferred introducing a sink term S_{solid} in the energy equation. This term, directly related to the compression rate, required only the adjustment of a constant κ.

$$S_{\text{solid}} = \kappa \frac{dp}{dt} \tag{10}$$

Boundary and initial conditions

Conservative heat flux condition was applied at the solid-liquid interface:

$$\left(\left(\lambda \vec{\nabla} T\right)_{\text{fluid}} - \left(\lambda \vec{\nabla} T\right)_{\text{solid}}\right) \cdot \vec{n} = 0 \tag{11}$$

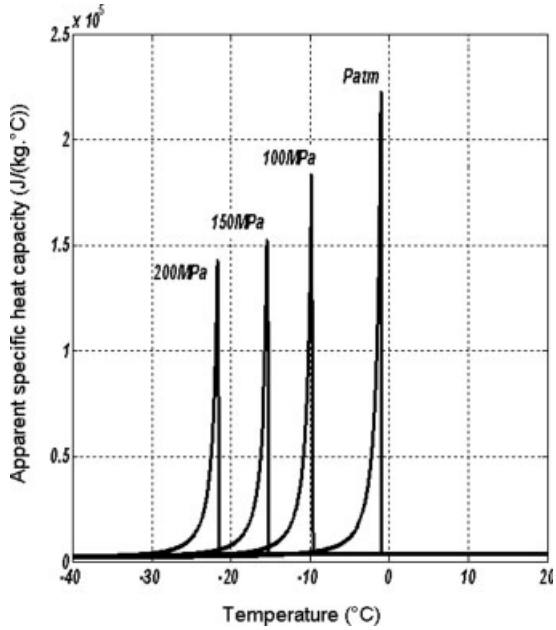

Figure 5. Evolution of the apparent specific heat capacity of Tylose according to the pressure and the temperature.

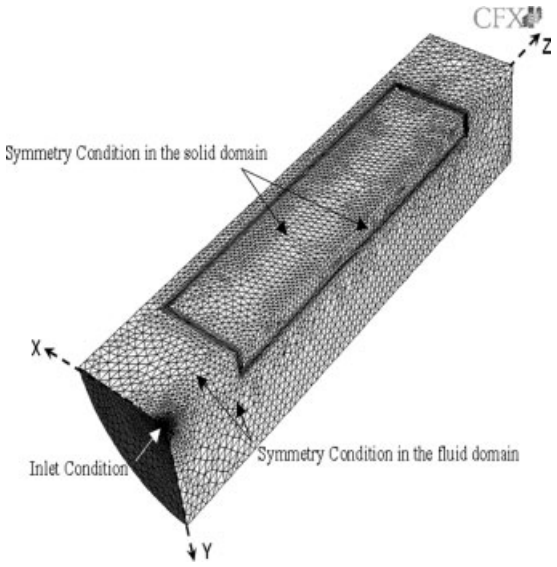

Figure 6. Boundary conditions and surface mesh of the fluid and solid domains.

It should be noticed that, as the code used a methodology proposed by Kader,[32] no local convection heat transfer coefficient was imposed. Whereas previous numerical contributions adjusted this parameter,[23–25] we calculated it afterwards. For the vessel walls and at the liquid–solid interfaces a no slip condition for the velocity was adopted.

Initial conditions were taken from the experimental device. The initial temperatures of the tylose and of the thawing medium (water) were respectively equal to -15 and 20°C. The water was considered initially stagnant, a zero velocity was considered in the whole domain.

During the process a constant temperature (20°C) was maintained on the internal walls of vessel. For symmetry reasons, a quadrant of the geometry was considered (Figure 6).

Preliminaries tests indicated that the injection velocity of 0.32 m s^{-1} permitted to reach 200 MPa at the end of the compression phase.

Numerical methods

A CFD code (CFX.5-7) was used to accommodate all these equations, initial, and boundary conditions. Fortran subroutines were designed and implemented in the model for thermophysical properties. We employed the second order upwind scheme of Rhie and Chow[33] in space and a second order scheme in time according to Patankar[34] and Norris.[35] A multigrid technique was used for the resolution of the linear system.

Results

Thawing medium

Figure 7a shows the pressure evolution measured during the process and the pressure calculated by the model. A very good agreement is observed between numerical and experimental data both during the rapid compression phase (80 s) and during the pressure holding phase. This is not trivial at all because the pressure is a variable that results from the mass flow rate injected in the vessel. A zero inflow condition was imposed at the end of the ramping period.

Figure 7b presents the temperature evolution at the middle and the top of the vessel. Experimental constraints did not permit to investigate with accuracy the fluid temperature at other locations. Nevertheless, the measurements give very interesting indications on the temperature evolution of the fluid. During the compression phase, up to 200 MPa, the temperature of water increases more than 2°C. As expected, the source term issued from an isentropic compression is suited to predict this temperature rise. During the holding phase, the heat transfer with the frozen sample provokes a cooling of the fluid which temperature finally tends towards the surrounding temperature. It appears that the cooling of the fluid is more important at mid-height than at the top of

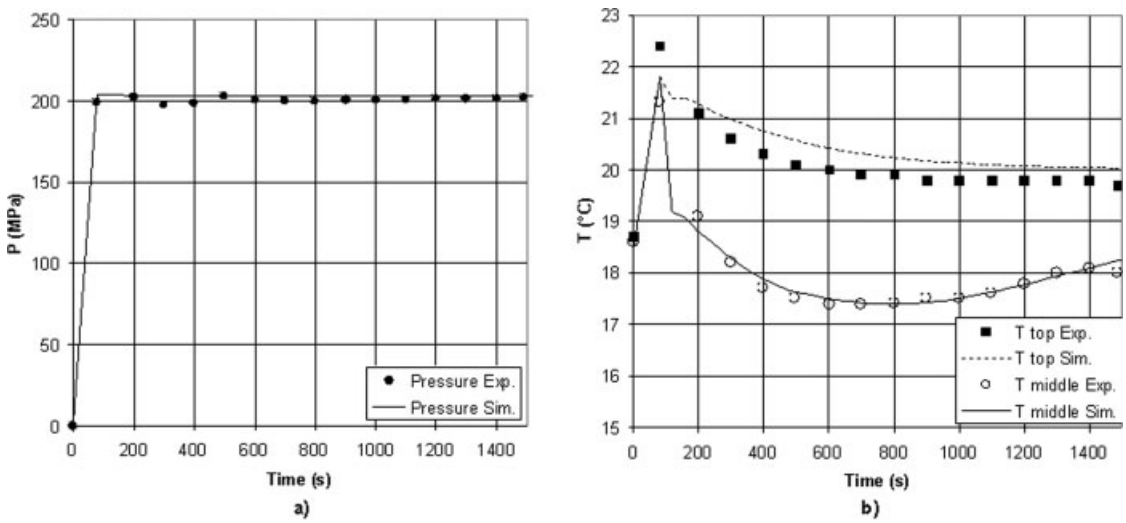

Figure 7. Experimental and numerical results in the pressure medium (a) pressure vs. time, (b) temperature in the vessel.

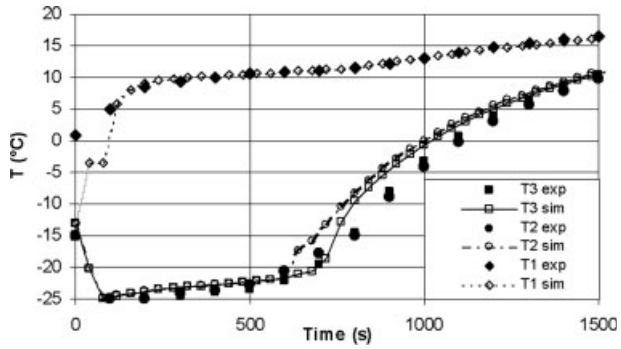

Figure 8. Experimental and calculated temperature profiles in the product, TEST 1.

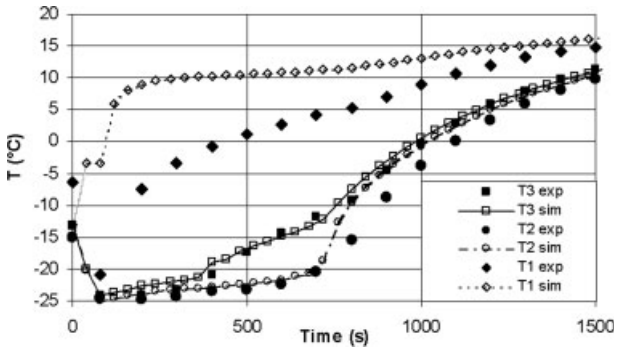

Figure 10. Experimental and calculated temperature profiles in the product, TEST 3.

the vessel. This is due to the convection phenomena that are further analyzed.

It is also noticeable that a very good agreement is observed between experimental and numerical results. It indicates that the flow pattern is well predicted. In previous studies carried out at atmospheric pressure, Ousegui et al.[26] conducted PIV experiments in order to validate the prediction of the velocity field by the model.

Phase change inside the food

Figures 8, 9 and 10 present the evolution of temperature inside the tylose for the three tests at 200 MPa. They allow a systematic comparison between the measurements and the predictions of temperature at three locations during the thawing processes. It should be noticed that the location of the tip of the thermocouples was not identical for each experiment. These curves point out three stages of the HP thawing process:

- a decrease of temperature during the compression phase (80 s).
- a pseudo temperature plateau corresponding to the phase change stage.
- a rapid temperature rise until reaching the vessel temperature.

The temperature profiles correspond very well with the computed temperatures, excepted for the thermocouple located close to interface in the third case (T3 on Figure 10). This difference is attributed to the experimental conditions.

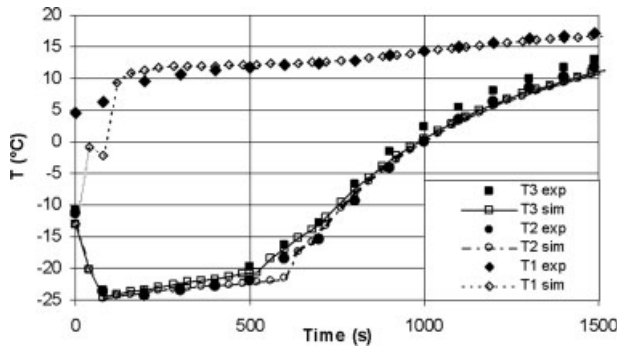

Figure 9. Experimental and calculated temperature profiles in the product, TEST 2.

In fact, measuring the temperature at the interface was not a simple task, the small decrease of temperature during the first times indicated that this thermocouple was few millimetres below the surface instead of being at the interface. Moreover, the installation of the sample and the connection of the thermocouples at the beginning of the experiments required nearly 3 min. This resulted in an imperfect control of the initial conditions, explaining the larger discrepancies observed at the surface locations.

At the other locations inside the food sample, temperature evolutions are perfectly predicted. During the compression and phase change stages (up to 600 s), errors are less than 0.5°C. If these errors could reach 5°C at the beginning of the temperature rise, they are greatly reduced to 0.5°C at the end of the process. This leads to an accurate prediction of the thawing times. These results demonstrate that the approach and the assumptions chosen to model this HP thawing process are efficient.

Discussion

As the model was validated, it was exploited to focus on the physical phenomena in the vessel. Several authors putted forward the uniform and rapid pressurization in the sample as well as in the vessel; this was considered by Knorr[36] as one of the major advantage of the HP treatment. The pressure distribution during the compression and holding phases are shown in Figure 11. This simulation permits to ensure the uniformity of the pressure in the vessel. In fact, a local scale is necessary to detect a vertical gradient of pressure corresponding to the hydrostatic pressure.

The velocity field in the vessel is presented at various stages of the process on Figure 12. During the compression stage (t = 80 s), the maximum velocity is reached at the section where water was injected (bottom of the vessel). As indicated by Hartmann et al.,[16] the flow is governed by forced convection during the compression phase. After this phase, we observe (t = 120 s) the decrease of the maximum velocity value and the displacement of this maximum toward the liquid–solid interface. The downward boundary layer and the recirculation phenomenon, which appears at the bottom of the vessel, are revealing the development of heat transfer by free convection. One can also observe in the upper locations a recirculation phenomenon caused by the temperature difference (2°C) between the wall of the vessel and the water

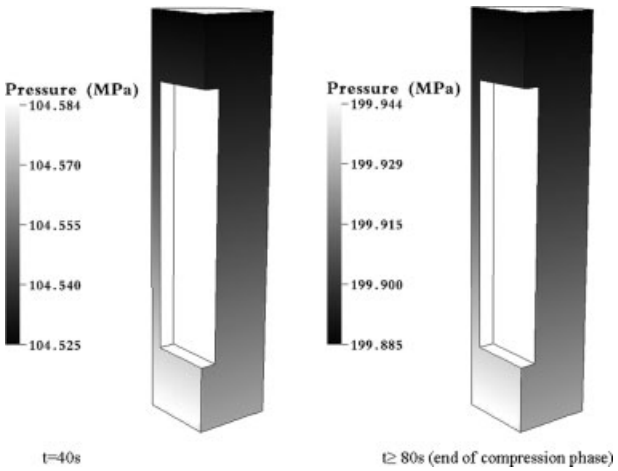

Figure 11. Pressure field inside the vessel during and at the end of the compression phase.

heated by compression (23°C at the end of the compression). The two last figures show the flow pattern at mid-term (t = 600 s) and at the end (t = 1200 s) of the thawing process. As the surface temperature does not evolve a lot during these stages, the driving force for natural convection is quasi-stable. The flow patterns look similar even if there is a slight decrease of the maximum value of velocity. One can notice the disappearance of the vortice at the top of the vessel. The flow then typically looks like the window-problem configuration with two opposite boundary layers separated by a stagnant fluid. These complex convective phenomena could not be taken into account using a single heat transfer coefficient between the surface and the fluid. An a posteriori calculation of an average heat transfer coefficient (integration over the whole interface) was performed (Figure 13). This average convective heat transfer coefficient between the solid and the fluid is not constant and considerably changes during the process. It reaches its maximum value (more than 330 W m^{-2} K^{-1}) during the forced convection regime at the end of the compression phase. Then, as the buoyancy forces decreases

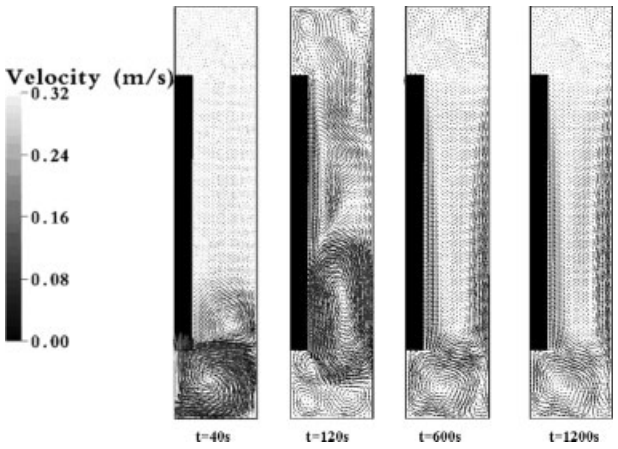

Figure 12. Velocity field during the principal phases of PIT process (final Pressure = 200 MPa).

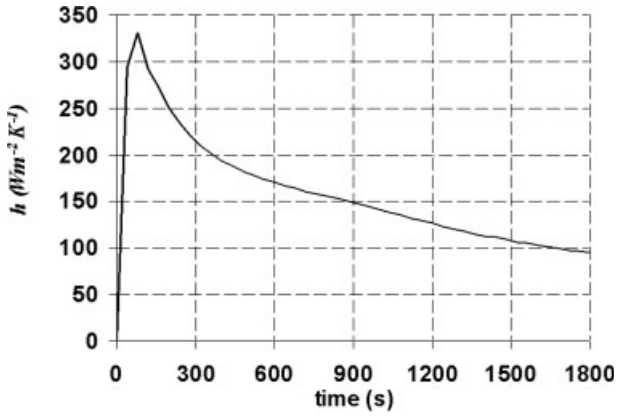

Figure 13. Evolution of the mean convective heat transfer coefficient.

during the holding phase it decreases toward a lower ending value (100 W m^{-2} K^{-1}). These values are of the same order than those deduced from a generalized correlation given for a three-dimensional body in an enclosure.[37]

To assess the influence of pressure on the thawing time, the thawing process of tylose was simulated at various pressures (from P_{atm} to 200 MPa by a step of 50 MPa). Figure 14 presents the predicted temperature profiles against time at the center of the product. The curves illustrate that the melting occurs at decreasing temperature with pressure and confirm the reduction of the thawing time with increasing pressure. This is in agreement with experimental data from Makita et al.[38] and Zaho et al.[5] If we consider the effective thawing time needed to reach 5°C, for low pressure a small difference is observed in comparison with the atmospheric pressure (10% for 50 MPa). For higher pressures, the thawing time decreases significantly, until reaching a reduction of 30% at 100 MPa. These percentages are similar to those proposed by Makita et al.[38]

Conclusion

In the present work, HP induced thawing process was studied and modeled by a CFD code with specific routines.

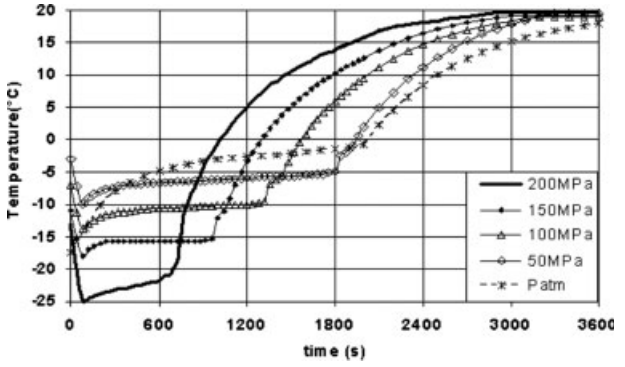

Figure 14. Temperature evolution in the center of the Tylose slab for different pressures.

The main novelty of this model lies in the fact that it takes into account the physical phenomena without any adjustement of a major governing parameter. The complex thermophysical properties function of pressure and temperature, both for the product and the fluid, were implemented. It allows the study of the natural convection phenomena in a compressible fluid during a transient process. To validate the model, experiments were conducted at 200 MPa in a pilot scale vessel. A good agreement between predicted and measured temperatures at different locations was observed, both in the solid and fluid domains. The results confirmed the effectiveness of the shift approach and the specific apparent heat capacity technique to model the phase change in biological products.

It was also demonstrated that the classical approach considering an apparent heat transfer coefficient between the vessel and the product was not appropriate to accurately predict the temperature evolution during HP process. In fact the convective heat transfer coefficient between the solid and the fluid domain was not constant and considerably changed during the process.

Moreover, the simulations proved that the flow in this kind of process considerably evolved. Forced convection was prevalent during the first stage of the process (compression), with a maximum velocity corresponding to the water injection. During the holding pressure stage, the natural convection was the prevalent heat transfer phenomenon in the pressurisation fluid domain. This phase was characterized by vortices at top and bottom locations of the vessel and by a displacement of the maximum fluid velocity toward the fluid-solid interface.

These complex flow phenomena tend to prove that such a model is required to investigate the HP thawing process at an industrial scale. This model should permit to determine the best way to achieve the optimal treatment of several products immersed in a large vessel.

Acknowledgments

This study was funded by the European Project Safe Ice (QLK1-CT-2002-02230). Luc Guihard and Christophe Couëdel are thanked for their technical support.

Notation

C_p = specific heat capacity (J kg^{-1} K$^{-1)}$
$\vec{g}$ = gravity (m s^{-2})
H = specific enthalpy (J kg^{-1})
p = pressure (Pa)
Q = volumetric thermal energy (J m^{-3})
S = source term (W m^{-3})
t = time (s)
T = temperature (K)
$\vec{V}$ = velocity vector (m s^{-1})
x, y, z = coordinates (m)
X = mass fraction (kg kg^{-1})

Greek letters

α = coefficient of thermal expansion (K^{-1})
κ = constant
λ = thermal conductivity (W m^{-1} K^{-1})
ρ = density (kg m^{-3})
μ = dynamic viscosity (Pa s^{-1})

Subscript

app = apparent
b = bounded water
fluid = fluid domain (water)
m = melting
solid = solid domain
wt = total water content

Literature Cited

1. Bridgman PW. Water in the liquid and five solid forms under pressure. *Proc Am Acad Arts Sci*. 1911;47:411–558.
2. Kalichevsky MT, Knorr D, Lillford PD. Potential food applications of high-pressure effects on ice-water transitions. *Trends Food Sci Technol*. 1995;6:253–259.
3. Urrutia Benet G, Schlueter O, Knorr D. High pressure low temperature processing. Suggested definitions and terminology. *Innovat Food Sci Emerg Technol*. 2004;5:413–427.
4. Fuchigami M, Teramoto A. Structural and textural changes in kinu-tofu due to high-pressure-freezing. *J Food Sci*. 1997;62;4:828–832.
5. Zaho YYR, Fores A, Olson DG. High hydrostatic pressure effects on rapid thawing of frozen beef. *J Food Sci*. 1998;63;2:272–275.
6. Hendrickx M, Ludikhuyze L, Van den Broeck I, Weemaes C. Effects of high pressure on enzymes related to food quality. *Trends Food Sci Technol*. 1998;9:197–203.
7. Martino MN, Otero L, Sanz PD, Zaritzky NE. Size and location of ice crystals in pork frozen by high-pressure-assisted freezing as compared to classical methods. *Meat Sci*. 1998;50;303–313.
8. Zhu S, LeBail A, Chapleau N, Ramaswamy H, de-Lamballerie-Anton M. Pressure shift freezing of pork muscle: effect on color, drip loss, texture and protein stability. *Biotechnol Prog*. 2003;20;939–945.
9. Knorr D, Schlueter O, Heinz V. Impact of high hydrostatic pressure on phase transitions of foods. *Food Technol*. 1998;52:42–45.
10. Cheftel JC, Levy J, Dumay E. Pressure-assisted freezing and thawing: principles and potential applications. *Food Rev Int*. 2000;16;453–483.
11. LeBail A, Chevalier D, Chourot JM, Monteau JY. High pressure calorimetry. Comparison of two systems (differential vs. single cell). Application to the phase change of water under pressure. *J Therm Anal Calorim*. 2001;66:243–253.
12. Li B, Sun DW. Novel methods for rapid freezing and thawing of foods—a review. *J Food Eng*. 2002;54:175–182.
13. Denys S, Van Loey AM, Hendrickx ME. A modeling approach for evaluating process uniformity during batch high hydrostatic pressure processing: combination of a numerical heat transfer model and enzyme inactivation kinetics. *Innov Food Sci Emerg Technol*. 2000;1:5–19.
14. Hartmann C, Delgado A. Numerical simulation of convective and diffusif transport effects on a high pressure induced inactivation process. *Biotechnol Bioeng*. 2002;79:94–104.
15. Hartmann C. Numerical simulation of thermodynamic and fluid-dynamic processes during the high-pressure treatment of fluid food systems. *Innov Food Sci Emerg Technol*. 2002;3:11–18.
16. Hartmann C, Schuhholz JP, Kitsubun P, Chapleau N, Le Bail A, Delgado A. Experimental and numerical analysis of the thermofluid-dynamics in a high-pressure autoclave. *Innov Food Sci Emerg Technol*. 2004;5:399–411.
17. Schluter O, Heinz V, Knorr D. Freezing of potato cylinders during high pressure treatment. In: Isaacs NS, editor. *High Pressure Food Science, Bioscience and Chemistry*. Cambridge UK: Royal Society of Chemistry, 1998:317–324.
18. Sanz P, Otero L. High pressure shift freezing. II. Modeling of freezing times for a finite cylindrical model. *Biotechnol Prog*. 2000;16:1037–1043.
19. Kowalczyk W, Hartmann C, Delgado A. Modelling and numerical simulation of convection driven high pressure induced phase changes. *Int J Heat Mass Trans*. 2004;47:1079–1089.
20. Bennon WD, Incropera FP. A continuum model for momentum, heat and species transport in binary solid-liquid phase change systems-I. Model formulation. *Int J Heat Mass Trans*. 1987;30:2161–2170.

21. Rattanadecho P. Simulation of melting of ice in a porous media under multiple constant temperature heat sources using a combined transfinite interpolation and PDE methods. *Chem Eng Sci*. 2006;61: 4571–4581.
22. Campañone L, Salvadori V, Mascheroni RH. Food freezing with simultaneous surface dehydration: approximate prediction of freezing time. *Int J Heat Mass Trans*. 2005;48:1205–1213.
23. Chourot JM, Boillereaux L, Havet M, LeBail A. Numerical modeling of high pressure thawing: application to water thawing. *J Food Eng*. 1997;34:63–75.
24. Denys S, Van Loey AM, Hendrickx ME, Tobback PP. Modeling heat transfer during high-pressure freezing and thawing. *Biotechnol Prog*. 1997;13:416–423.
25. Denys S, Van Loey AM, Hendrickx ME. Modeling conductive heat transfer during high-pressure thawing processes: determination of latent heat as a function of pressure. *Biotechnol Prog*. 2000;16:447–455.
26. Ousegui A, Le Bail A, Havet M. Numerical and experimental study of the thawing process by natural convection in an enclosure. *Am Inst Chem Eng J*. 2006;52:4240–4247.
27. Chizhov VE, Nagornov OV. Thermodynamics properties of ice, water and their mixture under high pressure. In: *the Proceedings of International Association of Hydrological Sciences Glaciers–Ocean–Atmosphere Interactions*, Wallingford (UK): IAHS Publisher, Vol. 208, 1991;463–470.
28. Schluter O. Impact of high pressure-low temperature processes on cellular materials related to food. PhD thesis, Berlin, Berlin University of technology, 2003.
29. Tanishita I, Nagaashima A, Murai Y. Correlation of viscosity, thermal conductivity and prandtl number for water and stream as a function of temperature and pressure. *Bull JSME*. 1971;14:1187–1197.
30. Miles CA. *The ice content of frozen meat and its measurement using ultrasonic waves. Meat freezing—why and how? MRI Symposium n 3, Langford, Bristol*, UK: Meat Research Institute, 1983.
31. Otero L, Ousegui A, Guignon B, Le Bail A, Sanz P. Evaluation of the thermophysical properties of tylose gel under pressure in the phase change domain. *Food hydrocolloids*. 2006;20:449–460.
32. Kader BA. Temperature and concentration profiles in fully turbulent boundary layers. *Int J Heat Mass Trans*. 1981;24:1541–1544.
33. Rhie CM, Chow WL. Numerical study of the turbulent flow past an airfoil with trailing edge separation. *AIAA J*. 1983;21:1525–1532.
34. Patankar SV. *Numerical Heat Transfer and Fluid Flow*. New York: Hemisphere, 1980.
35. Norris SE. A parallel navier-stokes solver for natural convection and free surface flow, PhD thesis, Departement of Mechanical Engineering, University of Sydney, 2000.
36. Knorr D. Effects of high-hydrostatic-pressure processes on food safety and quality, *Food Technol*. 1993;47;158–161.
37. Kakaç S, Shah RK, Aung W. *Handbook of Single-Phase Convective Heat Transfer*. New York: Wiley, 1987:13–41.
38. Makita T. Application of high-pressure and thermophysical properties of water to biotechnology. *Fluid Phase Equilibria*. 1992;76:87–95.

Appendix: Expression and Formulation of Thermophysical Properties of Water Under HP

Density

$$\rho(P,T) = \frac{\left[1 + m_2 \beta_{T_2} p\right]^{\frac{1}{m_2}}}{V_2^0(T)}$$

with:

$$\beta_{T_2} = \sum_{n=0}^{5} c_n (T - 273.15)^n \times 10^{-11} \quad \text{and}$$

$$V_2^0(T) = \frac{1 + b_1 \times (T - 273.15)}{\sum_{n=0}^{5} a_n (T - 273.15)^n} \times 10^{-3}$$

m_2	6.7
a_0	0.9998396
a_1	18.224944×10^{-3}
a_2	-7.922210×10^{-6}
a_3	-55.44846×10^{-9}
a_4	149.7562×10^{-12}
a_5	$-393.2952 \times 10^{-15}$
b_1	18.159725×10^{-3}
c_0	50.9804
c_1	−0.374957
c_2	7.21324×10^{-3}
c_3	-64.1785×10^{-6}
c_4	0.34302×10^{-6}
c_5	-0.684212×10^{-9}

T, temperature in K; p, pressure in bar.

Thermal expansion

$$10^4 \times \alpha(p,T) = A + \frac{B}{(C + \Pi)}$$

with:

$$A = \sum_{i=1}^{3} a_i T^{i-1}, \quad B = \sum_{i=1}^{3} b_i T^{i-1} + b_4 T + b_5 \Pi T;$$

$$C = \sum_{i=1}^{3} c_i T^{i-1}, \quad \Pi = \sum_{i=1}^{3} d_i p^{i-1}$$

a_1	47.8506
a_2	-8.12847×10^{-2}
a_3	8.49849×10^{-5}
b_1	5.56047×10^{5}
b_2	-3.76355×10^{3}
b_3	5.56395
b_4	5.59682×10^{-3}
b_5	−27.6522
c_1	-4.28067×10^{3}
c_2	-3.39150×10^{1}
c_3	3.65873×10^{-1}
d_1	-5.89618×10^{-4}
d_2	3.28892×10^{-4}
d_3	-2.65933×10^{-8}

T, temperature in K; p, pressure in bar.

Thermal conductivity

$$\lambda = 10^{-3} \times \sum_{i=0}^{2} D_i p^i$$

with:

$$D_0 = \sum_{i=0}^{4} D_{0i} \theta^i, \quad D_1 = \sum_{i=0}^{3} D_{1i} \theta^i, \quad D_2 = \sum_{i=0}^{2} D_{2i} \theta^i$$

D_{00}	0.568102×10^{3}
D_{01}	0.199947×10^{1}
D_{02}	-0.106453×10^{-1}
D_{03}	0.229461×10^{-4}
D_{04}	-0.391562×10^{-7}
D_{10}	0.946043×10^{-1}
D_{11}	-0.310186×10^{-3}
D_{12}	-0.205224×10^{-5}

D_{13}	0.189662×10^{-7}
D_{20}	-0.453755×10^{-4}
D_{21}	0.108352×10^{-5}
D_{22}	-0.544899×10^{-8}

θ, temperature in °C; p, pressure in bar.

Dynamic viscosity

Viscosity μ (Pa s^{-1})	a_1	a_2	a_3
$\mu^{-1} = a_1 + a_2\theta + a_3P^3$	609.73804	15.361378	-1.2739×10^{-6}

θ, temperature in °C; p, pressure in bar.

Specific heat capacity

Specific heat C_p (kJ/kg/°C)	a_1	a_2	a_3
$C_p = a_1 + a_2\theta + a_3p^{0.5} \times \ln(p)$	4.0501716	0.011311442	0.004858828

θ, temperature in °C; p, pressure in bar.

Manuscript received Jan. 25, 2007, and revision received Oct. 4, 2007.